RESEARCH ARTICLE

DOI: 10.1002/adsc.202((will be filled in by the editorial staff))

Understanding Chiral Proton Catalysis using Cinchonium Derivatives in aza-Michael Additions

Fernando Auria-Luna,[a] Eugenia Marqués-López,[a] M. Concepción Gimeno,[b] Juan V. Alegre-Requena[b]* and Raquel P. Herrera[a]*

[a] Laboratorio de Organocatálisis Asimétrica, Departamento de Química Orgánica, Instituto de Síntesis Química y Catálisis Homogénea (ISQCH) CSIC-Universidad de Zaragoza, C/ Pedro Cerbuna 12, 50009 Zaragoza, Spain. Phone: +34 976761190, email: raquelph@unizar.es

[b] Departamento de Química Inorgánica, Instituto de Síntesis Química y Catálisis Homogénea (ISQCH) CSIC-Universidad de Zaragoza, C/ Pedro Cerbuna 12, 50009 Zaragoza, Spain. Phone: +34 976761296, email: jv.alegre@csic.es

Received: ((will be filled in by the editorial staff))

Supporting information for this article is available on the WWW under http://dx.doi.org/10.1002/adsc.201######.((Please delete if not appropriate))

Abstract. This work presents a detailed mechanistic study of a quininium-catalyzed aza-Michael reaction, providing essential information for advancing chiral proton catalysis (CPC). The use of cinchona derivatives as chiral proton catalysts demonstrates their potential beyond their conventional roles as base-promoted and phase-transfer catalysts. Competitive reaction pathways are explored using density functional theory (DFT), wavefunction theory, and microkinetic simulations. Theoretical analyses are complemented with experimental titration and kinetic techniques to verify the intrinsic details of the reaction. This study reveals an intricate hydrogen bond network formed in the rate- and selectivity-determining step, involving four noncovalently attached components that favor a stronger substrate···catalyst interaction in the *R* transition state. Significantly, this research emphasizes the pivotal role of carboxylate anions as nucleophile-activating bases impacting reaction yield and enantioselectivity. Therefore, this work introduces cinchonium derivatives as new options for CPC and provides a thorough mechanistic analysis significant in expanding this underdeveloped catalytic domain.

Keywords: Chiral Proton Catalysis; Cinchonium derivatives; DFT calculations; Reaction Mechanism; aza-Michael reaction

Introduction

Chiral proton catalysis (CPC) is a field that relies on substrate activation through ionic hydrogen bonds, a concept labeled by Johnston and coworkers in 2004.[1] However, to date, it has been scarcely explored in the literature. This area, which is often included in the broader category of Brønsted acid catalysis,[2-6] encompasses chiral cationic catalysts that bear protonated nitrogen atoms serving as hydrogen-bond donors, preserving the protonation state after performing the catalytic cycles with no need to add any external reagent.[7-10] The increased acidity of charged hydrogen donors provides an advantage in the activation of electrophiles, as proton acidity is greater than that of common motifs used in organocatalysis, such as (thio)ureas, squaramides, and similar NH donor groups.[11-13]

Despite the great potential of CPC, the scarcity of available catalyst families enormously hinders the development of this area (Figure 1A).[1,14-19] Consequently, the number of studies regarding CPC remains far fewer than those of other areas of organocatalysis, and only a few reaction types, such as the aza-Henry,[20-26] Hetero-Diels–Alder,[27] and iodolactonization reactions,[28] have been considered. The main reasons behind the lack of progress in this area are probably related to the high complexity of CPC reactions, which often involve processes with four noncovalent units. In this sense, the absence of a solid mechanistic understanding of CPC delays any attempt to discover or improve new catalysts.

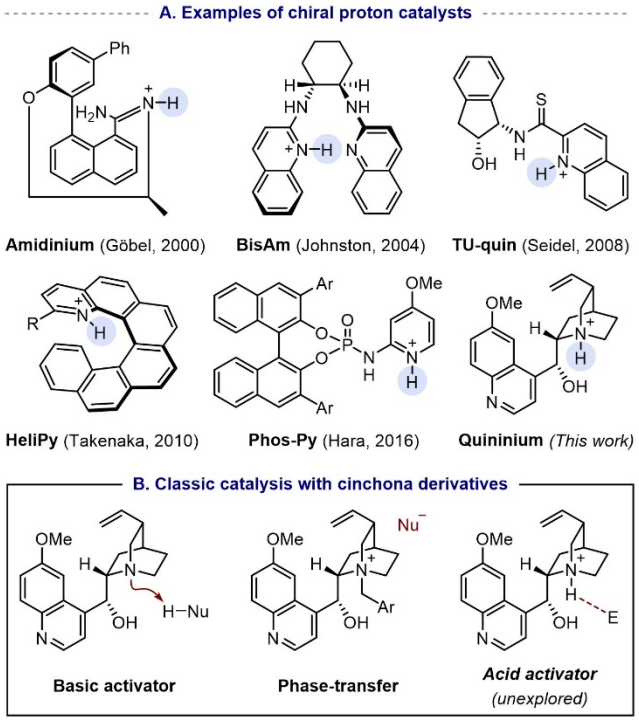

Figure 1. (A) Representative examples of families of chiral proton catalysts. (B) Roles of cinchona derivatives in catalysis.

To the best of our knowledge, there have only been a few computational studies attempting to rationalize the mechanism behind a CPC reaction.[29-33] The results confirm the high complexity of mechanistic studies in this type of catalysis, involving competitions between multiple transition states (TSs) and conformations, and the formation of extensive noncovalent interaction networks. Consequently, there is still an important gap of information regarding reaction mechanisms that needs to be filled to ensure optimal development of CPC reactions. For example, future research focused on CPC could benefit from experimental kinetic experiments aimed at revealing the rate- and selectivity-determining steps.

Furthermore, a good correlation between computational results, microkinetic simulations, and experimental rates and enantioselectivity is necessary to ensure that state-of-the-art theoretical methods are reliable enough to model CPC systems. These theoretical tools may play a crucial role in revealing elusive reaction details, such as the influence of counterions on enantioselectivity in CPC. Understanding the role of commonly ignored counteranions would uncover new features important for reaction development.

In this study, *N*-protonated cinchonium derivatives are presented as a new family of catalysts for promoting aza-Michael additions. The use of this family of compounds as chiral proton catalysts showcases their potential beyond their commonly recognized roles as base-promoted[34] and phase-transfer catalysts (Figure 1B).[35] We employ both computational and experimental techniques to comprehensively expand our mechanistic understanding of the studied reaction. This approach has the potential to offer valuable insights and facilitate the development of CPC.

Results and Discussion

Synthesis of catalysts and reaction development

Protonated cinchonium catalysts were prepared using an efficient and straightforward protocol that involves mixing equimolar amounts of cinchona alkaloids and Brønsted acids (Scheme 1). The catalysts can be obtained by evaporating the solvent and the synthetic method was compatible with different cinchona derivatives, such as quinine (**QN**, **1**) and cinchonidine (**CD**, **2**), and acids (**a-d**). The synthesis of the catalysts was confirmed through monocrystal X-ray diffraction analysis using **2b**, which revealed the presence of protonated quinuclidine groups in the cinchona derivatives.[36]

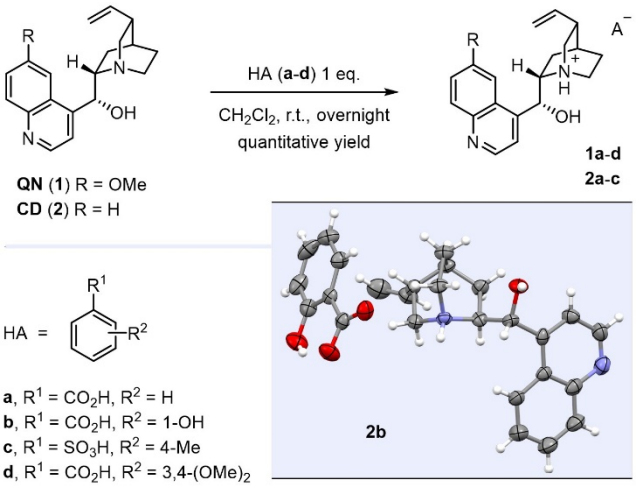

Scheme 1. Synthesis of cinchonium derivatives **1a-d** and **2a-c** and X-ray structure of compound **2b**.

The catalysts were tested in the target aza-Michael addition of hydrazides **3** to nitrostyrene derivatives **4**. After an extensive screening of reaction conditions, it was determined that the optimal conditions included catalyst **1d** and hydrazide **3c**, using CH_2Cl_2 as the solvent at –27 °C (Table S1). Additional tests were performed using individually **1**, benzoic acid, and sodium benzoate as catalysts for the reactions (Table S1, entries 27-29). The unsuccessful results obtained in the latest cases suggest that both parts of the cinchonium salts are necessary to promote optimal reactivity and enantioselectivity. Furthermore, the nuclear magnetic resonance (NMR) spectra of catalysts **1** and **2** indicate that their quinuclidine groups remain protonated in solution (Figure S9). As shown in Scheme 2, the aza-Michael addition was successfully implemented using different nitroalkenes **4**.

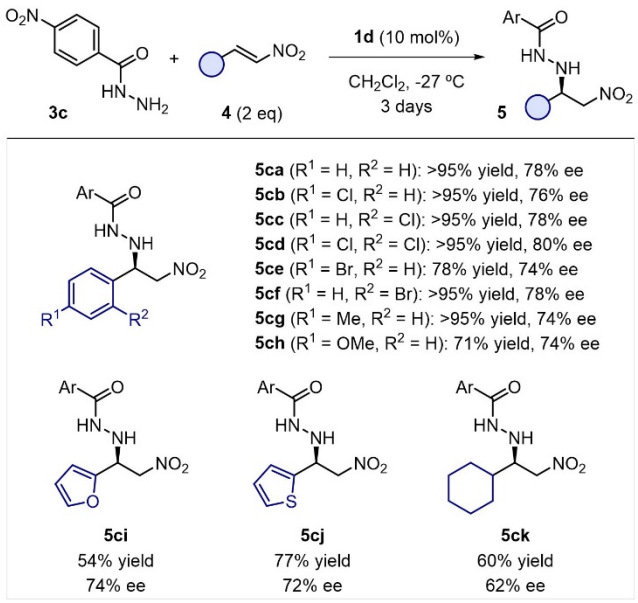

Scheme 2. Scope of the aza-Michael reaction catalyzed by **1d**.

In most cases, the final products **5** were obtained with excellent yields and good enantiomeric excesses (ee). As a general trend, the data suggests that the yield and ee increase as the nitroalkene acceptor becomes more electron-withdrawing (78 to >95% yield in **5ca-cg** *vs* 54 to 77% yield in **5ch-cj**). The absolute configuration of adducts **5** was determined to be *R* based on previous data.[37]

Computational mechanistic study

We first employed computational techniques to investigate the reaction mechanism using **1a**, **3c**, and **4a**. We modeled catalyst **1a** since this structure does not contain the two methoxy groups of **1d** while giving very similar yield and ee (Table S1, entries 23 and 24 *vs* 30 and 31). Multiple competitive pathways and activation modes were considered (Figure 2 and Figure S49), as well as an extensive conformational space[38] (see the Conformational sampling section of the ESI for more details).

Due to the differences in energy observed when varying the level of theory, we opted to include various DFT and wavefunction theory methods.[39-41] Figure 2 displays the energy deviations of eight combinations of widely used functionals and basis sets in modern mechanistic studies (yellow area, methods A to H, and Figure S50). The eight selected methods influenced geometry optimization, frequency calculations, and single-point energy corrections. The optimal method was selected based on its agreement with three different experimental measurements. The first two values were the energies of formation for reaction steps **1a**···**3c** and (*R*)-**Int-IV**, extracted from ^{1}H NMR titration experiments (Figure S48 and Table S5). Additionally, the benchmarking included the measured ee of the process (Table S6).

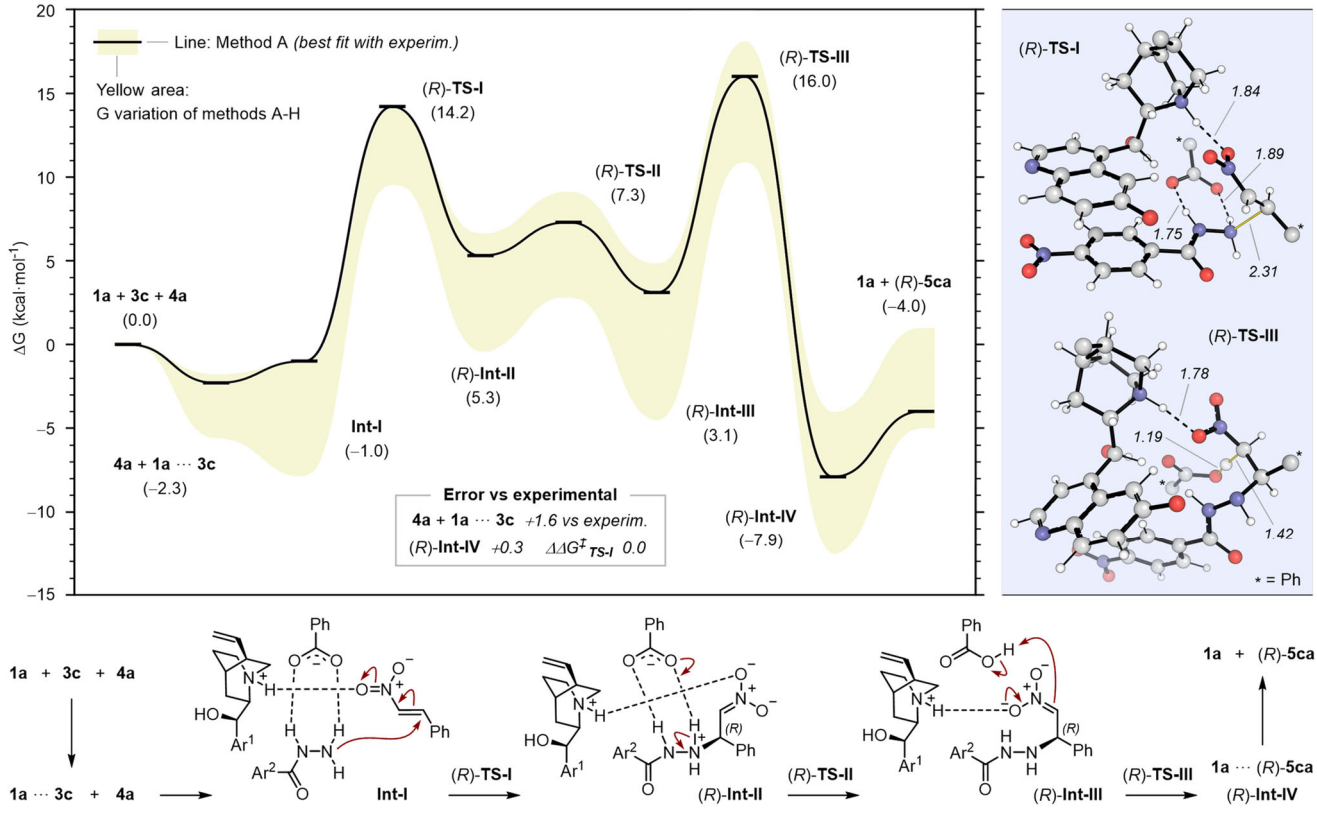

Figure 2. Energy profile using Boltzmann weighted ΔG values (in kcal·mol^{-1}) with catalyst **1a**, 4-nitrophenylhydrazide (**3c**), *trans*-*β*-nitrostyrene (**4a**), Ar1 = (6-methoxyquinoline-4-yl); Ar^2 = 4-NO$_2$-phenyl. Representations of the most stable conformers found in (*R*)-**TS-I** and (*R*)-**TS-III** with method A are also included. The most relevant H bonds are included as

dotted black lines and bonds involved in the TSs are shown as thin yellow lines. Distances are included in Å. Quasi-harmonic (QHA) vibrational, 1 M standard state and conformational entropy corrections were computed and applied by the GoodVibes[48] program at –27 °C (246.15 K). The SMD solvation model with dichloromethane was included in all the calculations. The levels of theory used are (A) ωB97X-D/Def2-QZVPP//ωB97X-D/6-31+G(d,p), (B) M06-2X-D3/Def2-QZVPP//ωB97X-D/6-31+G(d,p), (C) B3LYP-D3(BJ)/Def2-QZVPP//ωB97X-D/6-31+G(d,p), (D) ωB97X-D/6-311++G(2df,p)//ωB97X-D/6-31+G(d,p), (E) ωB97X-D/aug-cc-pVTZ//ωB97X-D/6-31+G(d,p), (F) DLPNO-CCSD(T)/cc-pV(DT)Z//ωB97X-D/6-31+G(d,p), (G) M06-2X-D3/Def2-QZVPP//M06-2X-D3/6-31+G(d,p) and (H) B3LYP-D3(BJ)/Def2-QZVPP//B3LYP-D3(BJ)/6-31+G(d,p). The yellow area represents the range of values from the eight methods.

Method A (ωB97X-D/Def2-QZVPP//ωB97X-D/6-31+G(d,p), SMD) exhibited superior performance compared to the three experimental values. This method showed low errors in Gibbs free energy (G) with discrepancies of only 1.6 and 0.3 kcal·mol^{-1} when compared to the experimental results of **1a···3c** and (*R*)-**Int-IV**, respectively (Table S5). Furthermore, the calculated and experimental ee values were found to be identical (1.0 kcal·mol^{-1} for both DFT and experimental values, Table S6).

The reaction proceeds through a relatively complex mechanism involving four noncovalently attached components. Reaction pathways containing four interacting units are rare in organocatalytic mechanistic studies,[42-47] typically only containing noncovalent catalytic clusters with up to three units of catalyst and substrate. The mechanism begins with the exergonic formation of the catalyst···hydrazide (**1a···3c**) and catalyst···hydrazide···nitrostyrene complexes (**Int-I**, Figure 2). Experimentally, the reaction does not proceed until all components are added, and no side products are formed. These observations suggest that reagents and initial noncovalent aggregates **1a···3c** and **Int-I** can interconvert before any transformation occurs.

Subsequently, the hydrazide nucleophile attacks nitrostyrene (**TS-I**), leading to the creation of the *R* stereocenter. Then, a rapid proton transfer occurs between the intermediate Michael adduct and the benzoate anion (**Int-II** to **Int-III**), followed by the protonation of the intermediate adduct in **TS-III**. The most stable species of the profile, the noncovalent catalyst···product complex observed in **Int-IV**, might cause catalyst inhibition as product **5ca** is generated. This effect has been previously observed in other cinchona-catalyzed reactions,[47] suggesting that it might not be a rare event in catalysis with cinchona derivatives.

The computational mechanism revealed an important interaction between the acidic quinuclidinium group and nitroalkenes **4**, which is likely the main activating interaction of the electrophiles during the **TS-I** addition. This interaction is also present in all the TSs of the reaction. Additionally, the results suggest that the benzoate counteranion forms H bonds that aid the nucleophilic attack of **3c** during the addition.

Experimental mechanistic study and validation of computational results

The theoretical results obtained are crucial to understand the mechanistic characteristics of the reaction. However, this computational insight requires experimental validation to ensure the validity of the proposed mechanism. One of the most important features to study through experimental kinetic experiments is the position of the rate-limiting step (RLS), as computational results show two potential candidates that are relatively close in energy (ΔG of 14.2 *vs* 16.0 kcal·mol^{-1} for (*R*)-**TS-I** and (*R*)-**TS-III**, respectively). Relying exclusively on these theoretical results to determine the RLS may be questionable due to the small energy difference between the two steps compared to DFT accuracy. For example, agreements of state-of-the-art DFT calculations with experimental barrier heights as high as 1.8 kcal·mol^{-1} per TS have been considered reasonably good even for simpler Diels-Alders and S_N2 reactions.[49] Therefore, the RLS was determined experimentally instead, using kinetic isotope effects (KIEs).

Two deuterated nitrostyrene derivatives were synthesized, which contained the D atom in different positions (Figure 3A). These deuterated compounds were designed to show specific KIEs in one of the two possible RLSs. First, **4a-β-D** contains the D atom in the position receiving the nucleophilic attack in **TS-I**. In this step, the deuterated C atom undergoes a hybridization change from sp^2 to sp^3, which is associated with inverse secondary KIEs.[50] In line with this prevision, the experimental values also showed secondary KIE effects of 0.91 with this substrate, suggesting that **TS-I** is the RLS.

In contrast, the D atom introduced in **4a-α-D** targets the hybridization change of the deuterated C atom involved in **TS-III**. The experimental results showed non-existent KIEs in this case (0.99), supporting the notion that **TS-I** is the RLS of the process. The calculated KIEs using DFT frequency information[51] also support that **TS-I** is the RLS in both substrates.

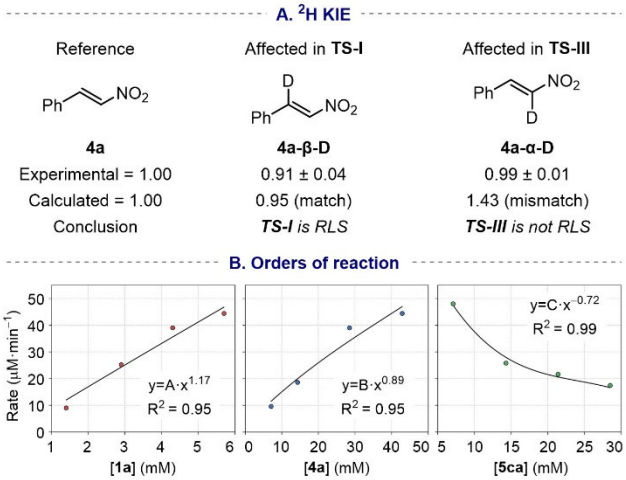

Figure 3. Experimentally observed KIEs (A) and orders of reaction (B).

We also used **4a-α-D** to study the reversibility of the overall process. The absence of D/H exchange in **5ca-α-D** over time indicates that the reaction is not reversible and the ee is determined in the RLS **TS-I**, implying kinetic control.

We then measured the orders of reaction (Figure 3B) to ensure proper design of the reaction pathways, in which only one molecule of each component is modeled. The order of reaction was measured for **1a** and **4a**, showing approximately order of one for each compound (1.17 and 0.89 for **1a** and **4a**, respectively) and matching the computational approaches. The negative order observed for **5ca** (–0.72) indicates that the reaction rate decreases as this product forms. This result is consistent with the favorable formation of complex **1a**···(*R*)-**5ca** observed in the computational profile ((*R*)-**Int-IV**, –7.9 kcal·mol^{-1}, Figure 2) and titration experiment (Figure S48).

Understanding stereoselectivity and reactivity

After validating the proposed energy profile through multiple kinetic studies, we directed our attention to the rate- and selectivity-determining step **TS-I** to analyze the key features influencing enantioselectivity. The structural analysis revealed a complex network of H bonds, in which the chiral proton activates the electrophile while the benzoate counteranion activates the nucleophile (Figures 4A and S51). Based on the Hammond-Leffler postulate[52,53] and the calculated reaction coordinates, the enhanced stabilization of the oxyanion in (*R*)-**Int-II** contributes to the earlier and lower activation barrier observed for this enantiomer (Figure 4B).

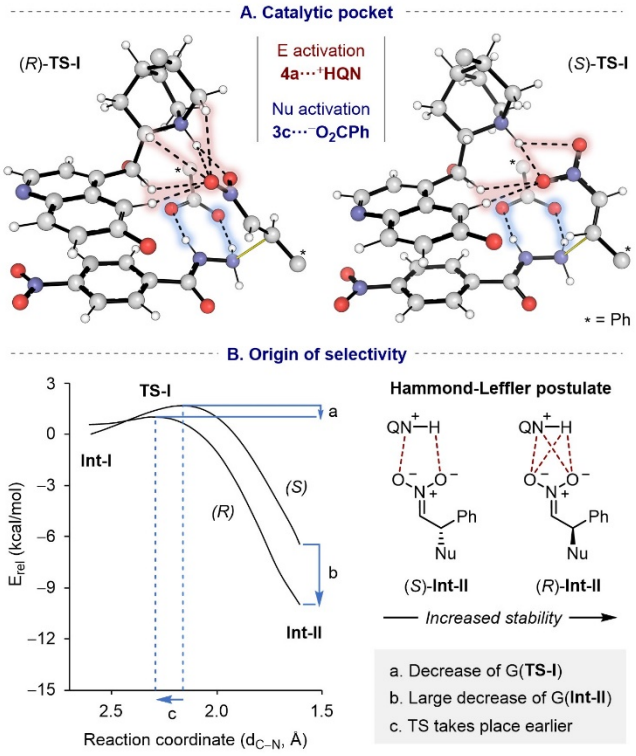

Figure 4. (A) Representation of the most stable conformers of (*R*)- and (*S*)-**TS-I**. Some non-participating groups were omitted for clarity. (B) Origin of enantioselectivity in **TS-I** studied with the intrinsic reaction coordinates of the most stable conformers, (*R*)-**TS-I**_24 and (*S*)-**TS-I**_1, at the optimization level.

The activation of both electrophile and nucleophile is also important for modulating reactivity. In this context, the chosen counteranion should not be regarded as innocuous, as it can impact reaction rates by interacting with the nucleophile in **TS-I**. We further tested this hypothesis using chloride as the anion (**1e**) since this change should trigger a diminished nucleophile activation caused by the poorer ability of chloride to form H bonds with hydrazide **3c** compared to benzoate. As expected, the calculations showed changes in the hydrogen bond networks that led to increased activation barriers (from **1a**···**3c** to (*R*)-**TS-I**, 16.0 *vs* 18.6 kcal·mol^{-1} for benzoate and chloride counteranions, respectively, Figure 5A), and the experimental yield dropped accordingly (from >95% to <10% for benzoate and chloride, respectively).

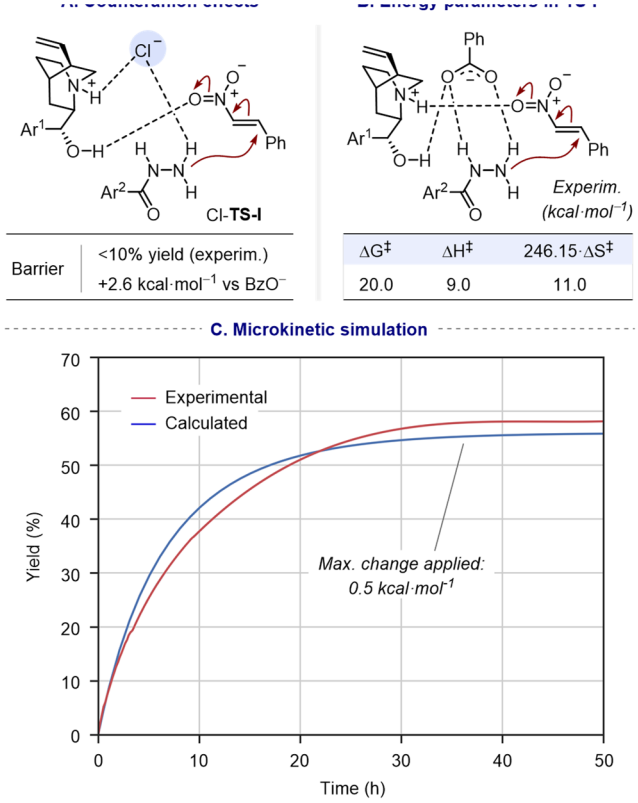

Figure 5. Calculated barrier and experimental yield obtained when using a catalyst with a Cl^- counteranion (**1e**) at –27 °C (246.15 K). (B) Experimental measurement of $\Delta G^‡$, $\Delta H^‡$ and $\Delta S^‡$. (C) Microkinetic simulation of the reaction using the computed averaged energy values *vs* an experimental profile. The reaction conditions were adjusted for NMR conditions and time: 0.01 mmol of **3c**, 0.01 mmol of **4a** and 0.003 mmol of **1a** in 0.6 mL CD_2Cl_2, T = 20 °C (293.15 K, G values recalculated at this T).

We next measured rate constants at different temperatures and prepared an Eyring plot (Figure S46) to calculate the activation parameters of the reaction (Figure 5B).[54] The results suggest that the entropic contribution prevails even at lower temperatures (9.0 *vs* 11.0 kcal·mol^{-1} at 246.15 K for $\Delta H^‡$ and $\Delta S^‡$, respectively). This observation is not surprising given that four noncovalently attached units participate in the calculated RLS.

A final microkinetic simulation[55] was performed to validate the calculated energy profile, comparing DFT and experimental results. This type of analysis is quite challenging and previous authors have allowed for deviations of up to 1.5 kcal·mol^{-1} in the energy of multiple DFT reaction steps.[56,57] Figure 5C shows that the experimental and predicted yield profiles over time match well when applying small changes of 0.5 kcal·mol^{-1} to the relative G values of only three reactions steps. The good agreement observed in this analysis further strengthens the theoretical mechanism.

Conclusion

In summary, we conducted a thorough investigation of a quininium-catalyzed aza-Michael reaction, which furnishes crucial data for developing reactions in CPC. The use of cinchona derivatives as chiral proton catalysts highlights their potential beyond their usual functions as base-promoted and phase-transfer catalysts. We used DFT, wavefunction theory, and microkinetic simulations to model competitive reaction pathways.

Different theoretical methods were included due to the high complexity of the mechanism, which involved four non-covalently interacting units. However, the close energy gaps between **TS-I** and **TS-III** made the determination of the RLS uncertain when relying solely on calculated results. Theoretical studies were complemented with experimental titration and kinetic techniques, which revealed that the rate- and selectivity-determining step was the hydrazide addition presented in **TS-I**. The experimental orders of reaction, with a value of one measured for **1a** and **4a**, reinforced the computational reaction profile used. Additionally, the negative order of reaction displayed by product **5ca** is in line with the favorable energy shown by **Int-IV** in the computational reaction profile. Further titration experiments provided additional support for this proposal.

The computational results suggest that a stronger substrate···catalyst interaction favors the *R* enantiomer in the selectivity-determining step **TS-I**. Computational and experimental tests also demonstrate how carboxylate counterions are crucial in understanding reaction yield and enantioselectivity, as they act as nucleophile-activating bases. Overall, this research introduces cinchonium derivatives as new options for CPC, accompanied by a comprehensive mechanistic study that could potentially broaden the scope of this underexplored area of catalysis.

Experimental Section

Details regarding the experimental procedures can be found in the supplemental experimental procedures.

Acknowledgements

The authors thank Agencia Estatal de Investigación (AEI/10.13039/501100011033, projects PID2020-117455GB-I00, PID2022-136861NB, PID2022-140159NA-I00 and PID2023-147471NB-I00) and Gobierno de Aragón-Fondo Social Europeo (Research Group E07_23R). The authors acknowledge the computing resources at the Galicia Supercomputing Center, CESGA, including access to the FinisTerrae supercomputer, and the Drago cluster facility of SGAI-CSIC.

References

[1] B. M. Nugent, R. A.Yoder, J. N. Johnston, *J. Am. Chem. Soc.* **2004**, *126*, 3418–3419.

[2] T. Akiyama, *Chem. Rev.* **2007**, *107*, 5744–5758.

[3] D. Kampen, C. M. Reisinger, B. List, *Top. Curr. Chem.* **2010**, *291*, 395–456.

[4] S. Schenker, A. Zamfir, M. Freund, S. B. Tsogoeva, *Eur. J. Org. Chem.* **2011**, 2209–2222.

[5] D. Parmar, E. Sugiono, S. Raja, M. Rueping, *Chem. Rev.* **2014**, *114*, 9047–9153.

[6]C. Min, D. Seidel, *Chem. Soc. Rev*. **2017**, *46*, 5889–5902.

[7] E. J. Corey, M. J. Grogan, *Org. Lett.* **1999**, *1*, 157−160.

[8] X. Fu, W.-T. Loh, Y. Zhang, T. Chen, T. Ma, H. Liu, J. Wang, C.-H. Tan, *Angew. Chem. Int. Ed.* **2009**, *48*, 7387−7390.

[9] K. Yoshida, T. Inokuma, K. Takasu, Y. Takemoto, *Synlett* **2010**, 1865−1869.

[10] A. L. Fuentes de Arriba, O. H. Rubio, L. Simón, V. Alcázar, L. M. Monleón, F. Sanz, J. R. Morán, *Tetrahedron: Asymmetry* **2017**, *28*, 819−823.

[11] A. S. Hess, R. A. Yoder, J. N. Johnston, *Synlett* **2006**, 147–149.

[12] G. Jakab, C. Tancon, Z. Zhang, K. M. Lippert, P. R. Schreiner, *Org. Lett.* **2012**, *14*, 1724–1727.

[13] X. Ni, X. Li, Z. Wang, J.-P. Cheng, *Org. Lett.* **2014**, *16*, 1786–1789.

[14] T. Schuster, M. Bauch, G. Dürner, M. W. Göbel, *Org. Lett.* **2000**, *2*, 179−181.

[15] M. Ganesh, D. Seidel, *J. Am. Chem. Soc.* **2008**, *130*, 16464−16465.

[16] K. Yoshida, T. Inokuma, K. Takasu, Y. Takemoto, *Molecules* **2010**, *15*, 8305−8326.

[17] N. Takenaka, J. Chen, B. Captain, R. S. Sarangthem, A. Chandrakumar, *J. Am. Chem. Soc.* **2010**, *132*, 4536−4537.

[18] W. Chen, W. Yang, L. Yan, C.-H. Tan, Z. Jiang, *Chem. Commun.* **2013**, *49*, 9854−9856.

[19] Y. Nishikawa, S. Nakano, Y. Tahira, K. Terazawa, K. Yamazaki, C. Kitamura, O. Hara, *Org. Lett.* **2016**, *18*, 2004−2007.

[20] A. Singh, R. A. Yoder, B. Shen, J. N. Johnston, *J. Am. Chem. Soc.* **2007**, *129*, 3466–3467.

[21] J. C. Wilt, M. Pink, J. N. Johnston, *Chem. Commun.* **2008**, 4177–4179.

[22] B. Shen, J. N. Johnston, *Org. Lett*. **2008**, *10*, 4397–4400.

[23] A. Singh, J. N. Johnston, *J. Am. Chem. Soc.* **2008**, *130*, 5866–5867.

[24] T. A. Davis, J. C. Wilt, J. N. Johnston, *J. Am. Chem. Soc.* **2010**, *132*, 2880–2882.

[25] B. Shen, D. M. Makley, J. N. Johnston, *Nature* **2010**, *465*, 1027–1032.

[26] T. A. Davis, M. W. Danneman, J. N. Johnston, *Chem. Commun.* **2012**, 5578–5580.

[27] D. J. Sprague, B. M. Nugent, R. A. Yoder, B. A. Vara, J. N. Johnston, *Org. Lett.* **2015**, *17*, 880–883.

[28] M. C. Dobish, J. N. Johnston, *J. Am. Chem. Soc.* **2012**, *134*, 6068–6071.

[29] L. Belding, S. M. Taimoory, T. Dudding, *ACS Catal.* **2015**, *5*, 343−349.

[30] S. M. Taimoory, T. Dudding, *J. Org. Chem.* **2016**, *81*, 3286−3295.

[31] C. Nájera, J. M. Sansano, E. Gómez-Bengoa, *Pure Appl. Chem.* **2016**, *88*, 561−578, and references therein.

[32] T. J. Struble, I. Smajlagic, H. Foy, T. Dudding, J. N. Johnston, *J. Org. Chem.* **2021**, *86*, 15606−15617.

[33] I. Smajlagic, J. N. Johnston, T. Dudding, *Chem. Eur. J.* **2023**, *29*, e202204066.

[34] G. S. Singh, E. M. Yeboah, *Rep. Org. Chem.* **2016**, *6*, 47–75.

[35] D. C. M. Albanese, M. Penso, *Eur. J. Org. Chem.* **2023**, *26*, e202300224.

[36] CCDC-2098237 (**2b**) Contains the supplementary crystallographic data for this paper. These data can be obtained free of charge via http://www.ccdc.cam.ac.uk/conts/retrieving.html (or from the CCDC, 12 Union Road, Cambridge CB2 1EZ, UK, Fax: +44 1223 336033, E-mail: deposit@ccdc.cam.ac.uk) .

[37] A. Alcaine, E. Marqués-López, R. P. Herrera, *RSC Adv.* **2014**, *4*, 9856–9865.

[38] S. Grimme, *J. Chem. Theory Comput.* **2019**, *15*, 2847–2862.

[39] M. J. Frisch, G. W. Trucks, H. B. Schlegel, G. E. Scuseria, M. A. Robb, J. R. Cheeseman, G. Scalmani, V. Barone, G. A. Petersson, H. Nakatsuji, *et. al.* (**2016)**. Gaussian 16 Revision B.01 (Gaussian, Inc.).

[40] J. V. Alegre-Requena, S. Sowndarya, R. Pérez-Soto, T. M. Alturaifi, R. S. Paton, *Wiley Interdiscip. Rev. Comput. Mol. Sci.* **2023**, *13*, e1663.

[41] F. Neese, *Wiley Interdiscip. Rev. Comput. Mol. Sci.* **2012**, *2*, 73–78.

[42] S. Maeda, S. Komagawa, M. Uchiyama, K. Morokuma, *Angew. Chem. Int. Ed.* **2011**, *50*, 644–649.

[43] R. Ramozzi, K. Morokuma, *J. Org. Chem.* **2015**, *80*, 5652–5657.

[44] Y. Park, K. C. Harper, N. Kuhl, E. E. Kwan, R. Y. Liu, E. N. Jacobsen, *Science* **2017**, *355*, 162–166.

[45] M.-S. Xie, B. Huang, N. Li, Y. Tian, X.-X. Wu, Y. Deng, G.-R. Qu, H.-M. Guo, *J. Am. Chem. Soc.* **2020**, *142*, 19226−19238.

[46] E. Gómez-Torres, D. A. Alonso, E. Gómez-Bengoa, C. Nájera, *Eur. J. Org. Chem.* **2013**, 1434–1440.

[47] I. G. Sonsona, J. V. Alegre-Requena, E. Marqués-López, M. C. Gimeno, R. P. Herrera, *Chem. Eur. J.* **2020**, *26*, 5469–5478.

[48] G. Luchini, J. V. Alegre-Requena, I. Funes-Ardoiz, R: S. Paton, *F1000Research* **2020**, *9*, 291.

[49] M. Bursch, J.-M. Mewes, A. Hansen, S. Grimme, *Angew. Chem. Int. Ed.* **2022**, *134*, e202205735.

[50] J. V. Alegre-Requena, E. Marqués-López, R. P. Herrera, *Chem. Eur. J.* **2017**, *23*, 15336–15347.

[51] Paton, R.S. KINISOT version 2.0.1 (Python adapted). Zenodo **2022**.

[52] J. E. Leffler, *Science* **1953**, *117*, 340–341.

[53] G. S. Hammond, *J. Am. Chem. Soc.* **1955**, *77*, 334–338.

[54] H. Eyring, *J. Chem. Phys.* **1935**, *3*, 107–115.

[55] R. Macey, G. Oster, T. Zahnley, Berkeley Madonna version 9.1.3 (University of California, Berkeley, **2018**).

[56] L. E. Rush, P. G. Pringle, J. N. Harvey, *Angew. Chem. Int. Ed.* **2014**, *53*, 8672–8676.

[57] A. Modak, J. V. Alegre-Requena, L. de Lescure, K. J. Rynders, R. S. Paton, N. J. Race, *J. Am. Chem. Soc.* **2022**, *144*, 86–92.

RESEARCH ARTICLE

Understanding Chiral Proton Catalysis using Cinchonium Derivatives in aza-Michael Additions

Adv. Synth. Catal. **Year**, *Volume*, Page – Page

Fernando Auria-Luna, Eugenia Marqués-López, M. Concepción Gimeno, Juan V. Alegre-Requena* and Raquel P. Herrera*